Revisiting structural phases in some perovskites: The case of math xmlns="http://www.w3.org/1998/Math/MathML">mrow>mi >Ba/mi>mi>Ce/mi>msub>mi mathvariant="normal">O/mi>mn>3/mn>/msub>/mrow>/ math>

Yali Yang, Hongjun Xiang, and Laurent Bellaiche

Phys. Rev. B **104**, 174102 — Published 1 November 2021

DOI: 10.1103/PhysRevB.104.174102

Revisiting structural phases in some perovskites: the case of $BaCeO_3$

Yali Yang,[1] Hongjun Xiang,[1] and Laurent Bellaiche[2,*]

[1]*Key Laboratory of Computational Physical Sciences (Ministry of Education), State Key Laboratory of Surface Physics, and Department of Physics, Fudan University, Shanghai 200433, China*

[2]*Physics Department and Institute for Nanoscience and Engineering, University of Arkansas, Fayetteville, Arkansas 72701, USA*

Abstract

An effective Hamiltonian is developed and used to investigate the different equilibrium phases that $BaCeO_3$ can possess, as a function of temperature. Such atomistic technique predicts that *monodomain* $BaCeO_3$ adopts a phase transition sequence that differs from the one commonly experimentally reported in this specific important perovskite, even if the end-members of this sequence (namely, the high-temperature cubic $Pm\bar{3}m$ state and the orthorhombic $Pbnm$ ground state) are identical between our simulations and measurements. In contrast with this experimental phase transition sequence, the predicted one is, in fact, in-line with a rule denoted here as "the gradual tilting rule" that guides the progressive change of oxygen octahedral tiltings about the three Cartesian axes from $Pm\bar{3}m$ to $Pbnm$. The fact that this rule is obeyed in many perovskites, along with some of our analyses and previous works, leads us to strongly suggest that intermediate phases experimentally reported in $BaCeO_3$ pertain to multidomains, twinning, and/or antiphase boundaries. Such suggestion should also apply to other perovskites for which the structural phase transition sequence does not follow "the gradual tilting rule".

I. INTRODUCTION

Perovskite systems possess the ABX_3 stoichiometry where A and B are both cations and X are anions such as O, F or I. They can exhibit useful properties, including ferroelectricity[1], piezoelectricity[2], magnetism[3], multiferroicity[4], superconductivity[5,6], optical response[7], etc., which make them intensively used in technologies and promising for novel devices and which also explains why they have been so much studied. At high temperature, they typically exhibit the ideal cubic perovskite $Pm\bar{3}m$ structure while lowering temperatures often results in new phases, including the orthorhombic $Pbnm$ state – which is the ground state that has been the most observed in perovskites[8]. One typical question to wonder is how perovskites transform from the high-temperature cubic $Pm\bar{3}m$ structure to this $Pbnm$ ground state, as the temperature is progressively reduced. To address such issue, it is useful to take advantage of the $a^{s_a}b^{s_b}c^{s_c}$ Glazer notations[9] that characterize tilting of the X_6 octahedra, and where a, b and c denote tilting about the three pseudo-cubic $< 100 >$ axes and s_a, s_b and s_c are symbols that can either be '0' to indicate no tiltings, '+' to symbolize in-phase tiltings and '-' to represent antiphase tiltings. For instance, the ideal cubic $Pm\bar{3}m$ structure is associated with the $a^0a^0a^0$ notation to indicate that no tilting exists about any of the symmetry-equivalent [100], [010] and [001] directions. On the other hand, the $Pbnm$ phase is assigned the $a^-a^-c^+$ notation to emphasize an antiphase tilting occurring about the [110] pseudo-cubic direction accompanied by in-phase tilting about the c-axis. So, how to go from $a^0a^0a^0$ to $a^-a^-c^+$, as perovskites are cooled down? Some possibilities are displayed in Fig. 1a and consist in the three different a, b and c axes adopting one after another, or sometimes at the same time, their tilting pattern associated with $Pbnm$ – which we will refer to as "the gradual tilting rule". For instance, as the temperature is reduced from high values, the c-axis can first adopt in-phase tiltings before both the a and b-axes decide to exhibit antiphase tilting. In this scenario, that has been, e.g., observed in $CsPbBr_3$, $CsPbCl_3$ and $NaMgF_3$ systems[10–12], the following transition sequence under cooling thus happens: $a^0a^0a^0 \rightarrow a^0a^0c^+ \rightarrow a^-a^-c^+$. One can also envision that antiphase tiltings about [110] occur before the in-phase tilting about [001] when the temperature is lowered, therefore giving the $a^0a^0a^0 \rightarrow a^-a^-c^0 \rightarrow a^-a^-c^+$ sequence[13]. Situations can be even more complex, but still consistent with gradual changes of the tiltings about the three axes towards the $a^-a^-c^+$ pattern. For instance, the $a^0a^0a^0 \rightarrow a^-a^0c^0 \rightarrow a^-a^-c^0 \rightarrow a^-a^-c^+$ transition sequence has

been reported in $SrZrO_3$[14], for which the antiphase tilting about the x-axis now occurs before the one about the y-axis. It can also happen that the intermediate $a^-a^-c^0$ disappears in that latter sequence, thus giving rise to $a^0a^0a^0 \rightarrow a^-a^0c^0 \rightarrow a^-a^-c^+$, as, e.g., found in in $CaTiO_3$[15,16]. Other complex possibilities within the "the gradual tilting rule" are (i) $a^0a^0a^0 \rightarrow a^-a^0c^0 \rightarrow a^-b^0c^+ \rightarrow a^-a^-c^+$, as, e.g., proposed in $SrHfO_3$[17] and for which the system now adopts $a^-b^0c^+$ before transforming to $a^-a^-c^+$; and (ii) $a^0a^0a^0 \rightarrow a^0a^0c^+ \rightarrow a^-b^0c^+ \rightarrow a^-a^-c^+$, as found in, e.g., $NaTaO_3$[18] and for which the system now possesses $a^0a^0c^+$ with in-phase tilting (rather than $a^-a^0c^0$ with antiphase tilting) before transforming into $a^-b^0c^+$ and then $a^-a^-c^+$. It also possible that some perovskites decide to directly go from $a^0a^0a^0$ to $a^-a^-c^+$ under cooling[19,20], which is also one solution of "the gradual tilting rule". Note that the structures assigned $a^-a^0a^0$, $a^0a^0c^+$, $a^-a^-c^0$ and $a^-b^0c^+$ tilting patterns in Fig. 1a are associated with $I4/mcm$, $P4/mbm$, $Imma$ and $Cmcm$ symmetries, respectively.

Strikingly, Figure 1b also indicates that there are two other reported possibilities to go from $a^0a^0a^0$ to $a^-a^-c^+$, but by violating "the gradual tilting rule" summarized in Fig. 1a. For instance, $a^0a^0a^0 \rightarrow a^-a^-a^- \rightarrow a^-a^-c^+$ has been reported in, e.g., Ref. [21] for $LaFeO_3$, in which the c-axis first prefers to have no tilting, then to adopt an antiphase tilting before "mysteriously" deciding to possess an in-phase tilting at lower temperatures. Here, the $a^-a^-a^-$ tilted structure is associated with the $R\bar{3}c$ symmetry. An even larger change of mind occurs in the $a^0a^0a^0 \rightarrow a^-a^-a^- \rightarrow a^-a^-c^0 \rightarrow a^-a^-c^+$ sequence indicated in Ref. [22] for $BaPrO_3$ and in Refs. [23,24] for $BaCeO_3$, for which now the c-axis first has no tilting, then acquires antiphase tiltings before they vanish once more and then are resuscitated but in in-phase fashion! One important material that exhibits such rather surprising sequence is thus $BaCeO_3$, which gains much attention due to its high ionic conductivity, making it relevant as electrolyte materials for solid oxide fuel cells, hydrogen pumps and sensors, and electrochemical reactors[25–27]. It also has a large lattice constant that makes it potentially useful as a substrate in order to induce tensile strain in epitaxial films made of perovskites with smaller lattice constants, and is one end-member of the intriguing $Ba(Ce,Ti)O_3$ relaxor system[28,29]. It is also interesting to realize that the value of the tolerance factor, which usually acts as an indicator of perovskite structures, seems to have no relationship with the adopted tilting paths. For instance, $SrZrO_3$, $SrHfO_3$, $LaFeO_3$, $BaCeO_3$ and $BaPrO_3$ all have a very similar tolerance factor (of 0.94 and 0.95)[30,31], while their tilting paths are different (see Fig. 1).

Since the reported $a^0a^0a^0 \rightarrow a^-a^-a^- \rightarrow a^-a^-c^0 \rightarrow a^-a^-c^+$ sequence in $BaCeO_3$ is puzzling and violates the gradual tilting rule, we decided to develop and use an atomistic effective Hamiltonian to investigate structural phases in $BaCeO_3$, at an atomistic level. Such numerical tool, that has been shown to be highly accurate in terms of phase transition sequence in many perovskites (see, e.g., Refs. [19,32–34]), predicts that, in fact, $BaCeO_3$ should rather adopt the "non-violating" $a^0a^0a^0 \rightarrow a^-a^0c^0 \rightarrow a^-a^-c^+$ sequence, *when in a monodomain form*. Analysis of its predictions, as well as some ideas expressed in some previous studies[35,36], strongly suggest that the reported $a^0a^0a^0 \rightarrow a^-a^-a^- \rightarrow a^-a^-c^0 \rightarrow a^-a^-c^+$ originates from the existence of different $a^-a^0c^0$ and $a^-a^-c^+$ multidomains in the macroscopic $a^-a^-a^-$ and $a^-a^-c^0$ intermediate phases, respectively.

The article is organized as follows. Section II describes the developed numerical scheme, while Section III reports its predictions. A discussion and suggestions about the relation between computational and experimental results are provided in Section IV. Finally, Section V concludes this article.

II. METHODS

Here, we develop an effective Hamiltonian (H_{eff}) to investigate properties of $BaCeO_3$ bulk. This H_{eff} possess four degrees of freedoms, that are: (1) the Ba-centered local soft modes $\boldsymbol{u}_i$, which are directly related to the electric dipoles of the 5-atom cells i [32]; (2) the Ce-centered pseudo-vectors $\boldsymbol{\omega}_i$ that characterize oxygen octahedral tiltings[34] in the 5-atom unit cells i. Note that the direction of $\boldsymbol{\omega}_i$ is the axis about which the oxygen octahedron of cell i rotates, while its magnitude is the angle, in radians, of such rotation; (3) the homogeneous strain tensor, to be denoted as $\{\eta_H\}$, with its zero corresponding to the equilibrium 0 K cubic state of $BaCeO_3$; and (4) Ce-centered dimensionless variables $\boldsymbol{v}_i$, that are linked to the inhomogeneous strain within the 5-atom cells i [32]. The analytical expression of the total internal energy of this effective Hamiltonian of $BaCeO_3$ is identical to that given in Refs. [19,33] for $NaNbO_3$ and $CsPbI_3$ (note that this expression has been successful to reproduce properties of these two latter complex materials, therefore demonstrating its validity). Consequently, the total internal energy is a sum of two different types of energies:

$$E^{\text{tot}} = E^{\text{FE}}(\{\boldsymbol{u}_i\}, \{\eta_l\}) + E^{\text{tilt}}(\{\boldsymbol{u}_i\}, \{\eta_l\}, \{\boldsymbol{\omega}_i\}) \quad (1)$$

where $E^{\rm FE}$ involves the local modes, elastic deformations and their interactions, and $E^{\rm tilt}$ includes the energies associated with oxygen octahedral tiltings and their couplings with strains and local modes (note that $\{\eta_l\}$ is the total strain, i.e., it includes both the homogeneous and inhomogeneous contributions).

$E^{\rm FE}$ gathers the following five terms, as initially indicated in Ref. [32]:

$$\begin{aligned} E^{\rm FE} = & E^{\rm self}(\{\boldsymbol{u}_i\}) + E^{\rm dpl}(\{\boldsymbol{u}_i\}) + E^{\rm short}(\{\boldsymbol{u}_i\}) \\ & + E^{\rm elas}(\{\eta_l\}) + E^{\rm int}(\{\boldsymbol{u}_i\},\{\eta_l\}), \end{aligned} \tag{2}$$

where $E^{\rm self}$ corresponds to the local mode self energy, $E^{\rm dpl}$ represents the long-range dipole-dipole interaction, $E^{\rm short}$ characterizes the short-range interactions between neighboring local modes excluding dipole-dipole interactions, $E^{\rm elas}$ is the elastic energy, and $E^{\rm int}$ represents the interaction between elastic deformation and local modes. Technically, we have

$$\begin{aligned} E^{\rm self} &= \sum_i \{\kappa_2 u_i^2 + \alpha u_i^4 + \gamma(u_{ix}^2 u_{iy}^2 + u_{iy}^2 u_{iz}^2 + u_{ix}^2 u_{iz}^2)\} \\ E^{\rm dpl} &= \frac{Z^{*2}}{\epsilon_\infty} \sum_{i<j} \frac{\boldsymbol{u}_i \cdot \boldsymbol{u}_j - 3(\hat{\boldsymbol{R}}_{ij} \cdot \boldsymbol{u}_i)(\hat{\boldsymbol{R}}_{ij} \cdot \boldsymbol{u}_j)}{R_{ij}^3} \\ E^{\rm short} &= \sum_{i \neq j} \sum_{\alpha\beta} J_{ij\alpha\beta} u_{i\alpha} u_{j\beta} \\ E^{\rm elas} &= \frac{N}{2} B_{11}(\eta_1^2 + \eta_2^2 + \eta_3^2) + N B_{12}(\eta_1\eta_2 + \eta_2\eta_3 + \eta_3\eta_1) \\ &\quad + \frac{N}{2} B_{44}(\eta_4^2 + \eta_5^2 + \eta_6^2) \\ E^{\rm int} &= \frac{1}{2} \sum_i \sum_{l\alpha\beta} B_{l\alpha\beta} \eta_l(\boldsymbol{R}_i) u_\alpha(\boldsymbol{R}_i) u_\beta(\boldsymbol{R}_i), \end{aligned} \tag{3}$$

where $\boldsymbol{R}_{ij} = \boldsymbol{R}_i - \boldsymbol{R}_j$, with $\boldsymbol{R}_i$ and $\boldsymbol{R}_j$ being the lattice vector of site i and j, respectively. The sums on i are done over all Ba-sites, and α and β are Cartesian components along the x-, y-, and z-axes. Furthermore, the sum on j in $E^{\rm dpl}$ is done over all the Ba-sites that are different from i, while that on $E^{\rm short}$ runs over the first, second and third nearest Ba neighbors of the Ba site i.

Note that the interaction matrix $J_{ij\alpha\beta}$ in $E^{\rm short}$ can be expressed in terms of different

nearest neighbor (NN) interactions as:

$$\begin{aligned}
\text{first NN: } J_{ij\alpha\beta} =& (j_1 + (j_2 - j_1)|\hat{\boldsymbol{R}}_{ij,\alpha}|)\delta_{\alpha\beta}; \\
\text{second NN: } J_{ij\alpha\beta} =& (j_4 + \sqrt{2}(j_3 - j_4)|\hat{\boldsymbol{R}}_{ij,\alpha}|)\delta_{\alpha\beta} \\
&+ 2j_5\hat{\boldsymbol{R}}_{ij,\alpha} \cdot \hat{\boldsymbol{R}}_{ij,\beta}(1 - \delta_{\alpha\beta}); \\
\text{third NN: } J_{ij\alpha\beta} =& j_6\delta_{\alpha\beta} + 3j_7\hat{\boldsymbol{R}}_{ij,\alpha} \cdot \hat{\boldsymbol{R}}_{ij,\beta}(1 - \delta_{\alpha\beta}),
\end{aligned} \tag{4}$$

where δ is the Kronecker symbol and $\hat{\boldsymbol{R}}_{ij,\alpha}$ is the α-component of $\boldsymbol{R}_{ij}/R_{ij}$.

Furthermore, the energy associated with oxygen octahedral tiltings and their interactions with the Ba-centered $\{\boldsymbol{u}_i\}$ local modes and strains is provided by the expression of Ref. [37], namely:

$$\begin{aligned}
E^{\text{tilt}}(\{u_i\}, \{\eta_l\}, \{\omega_i\}) =& \sum_i [\kappa_A\omega_i^2 + \alpha_A\omega_i^4 + \gamma_A(\omega_{ix}^2\omega_{iy}^2 + \omega_{iy}^2\omega_{iz}^2 + \omega_{ix}^2\omega_{iz}^2)] \\
&+ \sum_{ij}\sum_{\alpha\beta} K_{ij\alpha\beta}\omega_{i\alpha}\omega_{j\beta} + \sum_i\sum_\alpha K'\omega_{i,\alpha}^3\,(\omega_{i+\alpha,\alpha} + \omega_{i-\alpha,\alpha}) \\
&+ \sum_i\sum_{\alpha\beta} C_{l\alpha\beta}\eta_l(i)\omega_{i\alpha}\omega_{i\beta} \\
&+ \sum_{i,j}\sum_{\alpha,\beta} \mathrm{D}_{ij,\alpha\beta}u_{j,\alpha}\omega_{i,\alpha}\omega_{i,\beta} + \sum_{i,j}\sum_{\alpha\beta\gamma\delta} E_{\alpha\beta\gamma\delta}\omega_{i\alpha}\omega_{j\beta}u_{j\gamma}u_{i\delta}\ ,
\end{aligned} \tag{5}$$

for which the sums on i are all the Ce sites, and α and β are also Cartesian components along the x-, y-, and z-axes coinciding with the pseudocubic [100], [010], and [001] directions, respectively. The first sum of E^{tilt} has the onsite contributions related to the oxygen octahedral tiltings, as given in Refs. [37–40]. The second and third terms represent short-range interactions between oxygen octahedral tiltings, with j running over the Ce ions being first nearest neighbors of the Ce site i, as provided in Refs. [37] and [39] , respectively. $\omega_{i+\alpha,\alpha}$ in the third term is the α-component of the tilting-related pseudo vector at the site shifted from the Ce site i to its nearest Ce neighbor along the α axis. The fourth term of E^{tilt} characterizes the interaction between strain and tiltings, as given in Ref. [39]. The fifth and sixth terms describe the coupling between oxygen octahedral tiltings and local modes, that contain trilinear contributions (that are quantified by the $\mathrm{D}_{ij,\alpha\beta}$ parameters) and biquadratic terms (that are characterized by the $E_{\alpha\beta\gamma\delta}$ parameters). j runs over the eight Ba atoms that are first nearest neighbors of the Ce-site i in these fifth and sixth terms that were first provided in Refs. [37] and [39], respectively.

Note also that the $K_{ij\alpha\beta}$ parameters entering the second energy of $E^{\rm tilt}$ can be expressed as:

$$\text{first NN: } K_{ij\alpha\beta} = (k_1 + (k_2 - k_1)|\hat{\boldsymbol{R}}_{ij,\alpha}|)\delta_{\alpha\beta} \tag{6}$$

The parameters of $E^{\rm tot}$ for $BaceO_3$ are given in Table 1, and are extracted by conducting first-principle computations on relatively small cells (typically, up to 40 atoms). Practically, we use the generalized gradient approximation (GGA) within the revised Perdew-Burke-Ernzerhof functional (PBEsol)[41], as implemented in the VASP package[42], for these first-principle computations. The projector augmented wave (PAW)[42,43] is also applied to describe the core electrons, and we consider the Ba ($5s^25p^66s^2$), Ce ($4f^15s^25p^65d^16s^2$) and O ($2s^22p^4$) valence electrons with a 550 eV plane-wave cutoff.

The parameters of this $H_{\rm eff}$ are then used within Monte-Carlo (MC) computations on a $12 \times 12 \times 12$ supercell (which thus contains 8,640 atoms) at different temperatures. 40,000 MC sweeps are conducted for each considered temperature, with the first 20,000 sweeps allowing the considered bulk to reach its thermal equilibrium and the remaining 20,000 sweeps being used to obtain statistical averages. Note, as explained in more details below, we also performed a second set of calculations for which one single $H_{\rm eff}$ parameter differs from its first-principle value. This parameter is κ_A, and is taken as -0.208305 in this second set of computations (its *ab-initio* value is -0.138305, as indicated in Table 1).

In order to determine which structural phases are predicted from the effective Hamiltonian computations, we typically extract the following quantities from the outputs of the MC simulations at any investigated temperature: (1) the $< \omega_{\mathbf{R}} >$ vector that quantifies *antiphase*-tilting of the oxygen octahedra[34]. It is the statistical average (hence the $< ... >$ notation) of $\omega_{\mathbf{R}} = \frac{1}{N}\sum_i \omega_i(-1)^{n_x(i)+n_y(i)+n_z(i)}$, where the sum runs over the N sites i and $n_x(i)$, $n_y(i)$ and $n_z(i)$ are integers locating the cell i [this cell i is centered at $a_{lat}(n_x(i)\mathbf{x} + n_y(i)\mathbf{y} + n_z(i)\mathbf{z})$, with a_{lat} being the 5-atom cubic lattice constant]; (2) the $< \omega_{\mathbf{M}} >$ vector that characterizes *in-phase* oxygen octahedral tiltings and that is the statistical average of $\omega_{\mathbf{M}} = \frac{1}{N}\sum_i \omega_i(-1)^{n_x(i)+n_y(i)}$; (3) the $< \mathbf{u}_{\mathbf{X}} >$ vector that represents an antipolar vector (associated with the X-point of the cubic first Brillouin zone) and that is the statistical average of $\mathbf{u}_{\mathbf{X}} = \frac{1}{N}\sum_i \mathbf{u}_i(-1)^{n_z(i)}$; and (4) all six components of the homogeneous strain tensor, in Voigt notation[44]. Note that we also looked at the Fourier transform of the last MC configuration of both the local modes and tilting patterns[45] for each investigated

temperature, in order to be sure that other phases, that possess order parameters different from $< \omega_{\mathbf{R}} >$, $< \omega_{\mathbf{M}} >$ and $< \mathbf{u}_{\mathbf{X}} >$, are not found in our present H_{eff} simulations.

III. RESULTS

A. Results for first-principle-derived $\mathbf{H_{eff}}$ parameters

The aforementioned effective Hamiltonian with the *ab-initio* coefficients displayed in Table I predicts the ground state to be *Pbnm* (that is associated with the $a^-a^-c^+$ pattern in Glazer notations[9]), in agreement with experiments[23,24]. Figure 2(a) shows the temperature evolution of $< \omega_{\mathbf{R}} >$ and $< \omega_{\mathbf{M}} >$, when heating up $BaCeO_3$ from 10 K to 1200 K and using such effective Hamiltonian and parameters. Figure 2b and 2c display the concomitant behavior of $< \mathbf{u}_{\mathbf{X}} >$ and the components of the homogeneous strain, respectively. One can see that $BaCeO_3$ is predicted to remain in the orthorhombic *Pbnm* state up to 460 $\pm$ 10 K, as evidenced by (i) $< \omega_{\mathbf{R}} >$ being along the [110] pseudo-cubic direction and $< \omega_{\mathbf{M}} >$ being finite along the [001] pseudo-cubic direction, and (ii) $\eta_{H,3}$ being different from $\eta_{H,1} = \eta_{H,2}$, and $\eta_{H,6}$ being finite. As consistent with Figure 2(b), such *Pbnm* phase is also known to exhibit a finite antipolar vector, $< \mathbf{u}_{\mathbf{X}} >$, along [110] as a result of a trilinear coupling between $< \mathbf{u}_{\mathbf{X}} >$, $< \omega_{\mathbf{R}} >$ and $< \omega_{\mathbf{M}} >$ that energetically favors the stabilization of *Pbnm*[46] (Note that this antipolar vector and this trilinear coupling imply that realistic effective Hamiltonians should incorporate tiltings, local modes and their couplings, as done here. Such trilinear coupling is responsible for the hybrid improper ferroelectricity in some perovskite superlattices, and Ruddlesden-Popper type perovskites[47–49]). These three latter quantities decrease in magnitude as the temperature is increased from 0 K to 460 K within this *Pbnm* state. At $\simeq$ 470 K, $BaCeO_3$ undergoes a first-order transition to a tetragonal $I4/mcm$ phase, which corresponds to $a^-a^0a^0$ in Glazer notations[9], as $< \omega_{\mathbf{R}} >$ now only adopts a finite x-component while $\eta_{H,1}$ is now smaller in magnitude than $\eta_{H,2} = \eta_{H,3}$ and all shear strain components now vanish (note that our predicted $a^-a^0a^0$ phase has antiphase tilting as a result of the positive sign of the k_2 parameter indicated in Table 1). Such tetragonal $I4/mcm$ phase exists between 470 $\pm$ 10 K and 840 $\pm$ 20 K, with the antiphase oxygen octahedral tilting about the x-axis continuously decreasing from $\simeq$ 0.19 to 0 radians (or equivalently, from 10.8 to 0 degrees) when increasing the temperature within this range.

At 840 ± 20 K, $BaCeO_3$ then transforms into the cubic $Pm\bar{3}m$ state, for which $< \omega_{\mathbf{R}} >$, $< \omega_{\mathbf{M}} >$, $< \mathbf{u}_{\mathbf{X}} >$ and the shear strain components ($\eta_{H,4}$, $\eta_{H,5}$, $\eta_{H,6}$) all vanish, while $\eta_{H,1} = \eta_{H,2} = \eta_{H,3}$ are still finite but now equal to each other. $BaCeO_3$ adopts such cubic state for any temperature above 840 ± 20 K, according to our effective Hamiltonian and its first-principle coefficients.

The predicted low-temperature $Pbnm$ and high-temperature $Pm\bar{3}m$ structural phases are precisely those known experimentally in $BaCeO_3$[23,24]. However, the intermediate $I4/mcm$ state differs from the frequently reported rhombohedral $R\bar{3}c$ and orthorhombic $Imma$ in $BaCeO_3$, that correspond to $a^-a^-a^-$ and $a^-a^-a^0$ patterns, respectively[9]. In fact, the predicted $Pbnm \rightarrow I4/mcm \rightarrow Pm\bar{3}m$ transition sequence under heating has been reported in $CaTiO_3$[15,16], but never in $BaCeO_3$, to the best of our knowledge. Moreover, the computed transition temperatures also differ from the measured ones since, e.g., the cubic phase is known to first occur around $\simeq$ 1170 ± 20 K in $BaCeO_3$[23,50] rather than the 840 ± 20 K value seen in Figs. 2. The effective Hamiltonian technique can indeed lead to such quantitative discrepancy with experiments for transition temperatures, but a qualitative disagreement with measurements for the phase transition sequence is atypical, as, e.g., demonstrated in Refs. [32–34] for $BaTiO_3$ or even the complex $NaNbO_3$ and $Pb(Zr,Ti)O_3$ systems.

B. Results for modified $\mathbf{H_{eff}}$ parameters

In order to be sure that this quantitative discrepancy for the transition temperatures' values and qualitative disagreement for the phase transition sequence are not linked to each other, we decided to run the MC simulations again but by modifying a single H_{eff} parameter (namely κ_A from -0.138305 to -0.208305), in order to basically reproduce the lowest temperature at which the cubic phase appears. The resulting predictions for $< \omega_{\mathbf{R}} >$, $< \omega_{\mathbf{M}} >$, $< \mathbf{u}_{\mathbf{X}} >$ and $\{\eta_H\}$, as a function of temperature and when heating $BaCeO_3$ from its orthorhombic $Pbnm$ ground state, are displayed in Figs. 3. One can see that the phase transition sequence is precisely the same one as in Figs. 2 but the transition temperatures have indeed increased: the $Pbnm \rightarrow I4/mcm$ transition still has a first-order nature but is now happening at 580 ± 5 K, and the $I4/mcm \rightarrow Pm\bar{3}m$ phase transition is still of second-order but now occurs at 1130 ± 30 K. In fact, we played with several parameters of this effective Hamiltonian and never found a $R\bar{3}c$ state in-between the high-temperature

$Pm\bar{3}m$ and low-temperature $Pbnm$ phases. One may thus wonder if the phase transition sequence depicted in Figs. 2 and 3 is, in fact, the qualitatively correct one. A discussion is needed to explain such hypothesis, with emphasis on four questions/issues to be indicated and tackled next.

IV. DISCUSSION AND INTERPRETATION OF EXPERIMENTAL RESULTS

A. Can it be that there are multidomains in the measured phases?

To answer this question, let us pay attention to the $< \omega_{\mathbf{R}} >$ and $< \omega_{\mathbf{M}} >$ pseudo-vectors predicted at 473 K in Fig. 3a, for which the equilibrium state is $Pbnm$ (that has the $a^-a^-c^+$ tilting pattern). $< \omega_{\mathbf{R}} >$ has x- and y-components both equal to 0.152 radians, which are therefore equal to 8.70 degrees each. Strikingly, such value is very close to the 8.54 degrees reported for the antiphase tilting of oxygen octahedra about both the x and y axes in the $Pbnm$ state at that temperature[24], which demonstrates that the effective Hamiltonian can be highly accurate. Another proof of its accuracy is the values of the predicted a, b and c lattice constants (that are obtained from the strains depicted in Fig. 3c) equal to 6.20, 6.17 and 8.72 Å at 473 K, respectively, which compare well (within less than 0.9%) with the corresponding experimental data of 6.25, 6.23 an 8.79 Å of Ref. [24]. On the other hand, the predicted $< \omega_{\mathbf{M}} >$ has a z-component of 0.121 radians, which translates into a 6.9 degree and is therefore higher than the experimental in-phase oxygen tilting of 4.64 degree[24]. Such comparison already hints that there may be domains forming in $BaCeO_3$ that, for instance, have the same antiphase tilting patterns but opposed in-phase tiltings – hence leading to suppressed reported (macroscopic) in-phase tilting of oxygen octahedra. Such possibility is further emphasized by the experimental work of Ref. [35] discussing twin walls in the $Pbnm$ state of $BaCeO_3$.

B. What can the experimental $Imma$ ($a^-a^-a^0$) state then be?

Following such idea of suppression, one can then envision that the reported $Imma$ state, having an $a^-a^-a^0$ Glazer notation, is in fact made of different $Pbnm$ states (having similar $< \omega_{\mathbf{R}} >$ but opposed $< \omega_{\mathbf{M}} >$) that fully cancel, in average, the in-phase tiltings. Such possibility is reinforced when realizing that (i) the computed $< \omega_{\mathbf{R}} >$ of Fig. 3 at 573 K

(which is a temperature for which we predict $a^-a^-c^+$ in Fig. 3 while measurements indicate the $a^-a^-a^0$ pattern) has x- and y-components equal to 0.148 radians for our $a^-a^-c^+$ state, which thus gives an angle of 8.5 degrees and which is therefore close to the experimental value of 8.22 degrees about the x- and y-axes given in Ref. [24] for the $a^-a^-a^0$ phase; (ii) the calculated $< \omega_{\mathbf{M}} >$ of Fig. 3 at 573 K is within a temperature range for which this in-phase tilting is very sensitive to the temperature and deviates from a linear relation with such temperature, in contrast with its behavior below 400 K; and (iii) the (a, b, c) lattice constants measured in Ref. [24] for the $Imma$ state at 573 K are basically identical to those reported for the $Pbnm$ state at 473 K, namely (6.26, 6.23, 8.80) Å *versus* (6.25, 6.23, 8.79) Å– which is also consistent with our predicted values of (6.20, 6.18, 8.72) Å at 573K and (6.20, 6.17, 8.72) Å at 473 K both within the $Pbnm$ phase. Note that this proposed hypothesis of coexisting multidomains cancelling the averaged in-phase tiltings in $BaCeO_3$ is fully consistent with the idea of phase-transformation-induced twinning, and antiphase boundaries, expressed in Ref. [36], and can also explain why the reported $Pbnm \rightarrow Imma$-phase transition is of second-order in $BaCeO_3$[24,51]. This idea is also reminiscent of the recent computational and experimental suggestions that some macroscopic phases reported in other perovskites and that are structurally different from $Pnma$ (e.g., $a^0a^0c^+$ in $CsPbI_3$ and other hybrid perovskites) in fact arise from fluctuations between different $Pnma$ domains having opposed patterns for some of their tiltings[19,52,53].

C. What can the experimental $R\bar{3}c$ ($a^-a^-a^-$) state then be?

It is first worthwhile to realize that the observed phase transition between $Imma$ and $R\bar{3}c$ has been determined to be of first-order while, at higher temperature, $R\bar{3}c$ was experimentally determined to transform into $Pm\bar{3}m$ via a continuous, second-order phase transition. Such features bear a strong analogy with our first-order transition between $Pbnm$ and $I4/mcm$, and the second-order nature of the transition between $I4/mcm$ and cubic $Pm\bar{3}m$ predicted in Figs. 2 and 3. Consequently, one can advance the idea that the reported $R\bar{3}c$ state arises from the coexistence of different $I4/mcm$ states, e.g., with $a^-a^0a^0$, $a^0a^-a^0$ and $a^0a^0a^-$ Glazer patterns, resulting in an average effective $a^-a^-a^-$ pattern. Such possibility is emphasized by the facts that (i) experiments report at 773 K a tilting angle of 6.05 degrees about each of the x-, y- and z-axes in the $R\bar{3}c$ state, which therefore corresponds to a

total antiphase rotation of 10.48 degrees, or equivalently, 0.18 radians, while our calculated $< \omega_{\mathbf{R}} >$ of Fig. 3a has a similar magnitude of 0.19 radians in our $a^-a^0a^0$ phase at 773 K; and (ii) our computed (a, b, c) lattice constants at 773 K for the $I4/mcm$ phase are (6.229, 6.164, 6.164) Å, therefore giving an average lattice constant of about 6.19 Å which differs only by about 0.9% from the lattice constant of 6.24 Å experimentally determined in Ref. [24] within the $R\bar{3}c$ state. Once again, this possibility is in-line with the previously proposed existence of twin domains in $BaCeO_3$[35,36,54]. It may also be consistent with the fact that Raman studies in $BaCeO_3$ suggested a tetragonal phase (which is the crystallographic system of $a^-a^0a^0$)[55,56] rather than a rhombohedral state (which is the symmetry of $R\bar{3}c$) as neutron diffractions did for similar temperatures[23,24], since Raman has the tendency to probe *local* structures while diffractions provide *macroscopic* information.

D. Continuity of the phase transition sequence

Let us note here that our presently predicted $Pm\bar{3}m$ ($a^0a^0a^0$) $\rightarrow$ $I4/mcm$ ($a^-a^0a^0$) $\rightarrow$ $Pbnm$ ($a^-a^-c^+$) sequence as the temperature decreases proceeds by gradual steps in the tilting patterns, since an antiphase tilting first happens about the x-axis in the $I4/mcm$ state before an antiphase tilting then forms about the y-axis at the same time than an in-phase tilting occurs about the z-axis in the $Pbnm$ phase. On the other hand, the experimentally reported $Pm\bar{3}m$ ($a^0a^0a^0$) $\rightarrow$ $R\bar{3}c$ ($a^-a^-a^-$) $\rightarrow$ $Imma$ ($a^-a^-a^0$) $\rightarrow$ $Pbnm$ ($a^-a^-c^+$) upon cooling is rather mysterious since the tilting about the z-axis is first of antiphase nature in $R\bar{3}c$, then is annihilated in $Imma$ before "resuscitating" but now in in-phase fashion in the $Pbnm$ state (in other words, the predicted phase transition sequence obeys "the gradual tilting rule" mentioned in the introduction, while the experimental one does not). The presently proposed ideas that $Imma$ is in fact made of different $Pbnm$ domains and that $R\bar{3}c$ is a state resulting from the coexistence of several $I4/mcm$ domains allow such "mystery" to be resolved. Experimentally, one possibility may be to look at the symmetry of each domain within the grown samples, in order to confirm our predictions.

V. SUMMARY

In summary, we developed and used an atomistic effective Hamiltonian to shed some light into the reported $a^0a^0a^0 \rightarrow a^-a^-a^- \rightarrow a^-a^-c^0 \rightarrow a^-a^-c^+$ phase transition sequence of the important $BaCeO_3$ material, as the temperature is reduced. In particular, our goal was to understand why this sequence violates "the gradual tilting rule", since the tilting about the *c*-axis is (1) first null at high temperature, then is in (2) antiphase before (3) vanishing again when cooling the system, and then finally (4) being in-phase in the ground state. Items (2), (3) and (4) appear to be contradictory to each other since it will mean that interaction between tiltings about the z-axis would prefer to generate antiparallel alignment of such tiltings along any [001] line, no preferential organization between such tiltings and parallel alignment, respectively – while only one of these three solutions should physically occur at finite temperature once such tilting condenses on a long-range order because they are all associated with the same parameter which has a definite sign (these three solutions will correspond to such parameter being positive, null and negative, respectively). In fact, our numerical scheme predicts that $BaCeO_3$ should rather adopt a sequence that does satisfy "the gradual tilting rule", namely $a^0a^0a^0 \rightarrow a^-a^0a^0 \rightarrow a^-a^-c^+$ (which has been seen in other perovskites[15]), *if only a monodomain exists at any temperature*. Based on further analysis of our results, comparison with experimental data and hints provided in previous other works[35,36], we further invoke the possibility that the observed $a^-a^-a^-$ is made of several domains (each being of $a^-a^0a^0$-type, that is $a^-a^0a^0$, $a^0a^-a^0$ and $a^0a^0a^-$) while the reported $a^-a^-c^0$ consists of $a^-a^-c^+$ domains made of opposite in-phase tiltings about the *c*-axis. We hope that this possibility of multidomains will be tested soon in $BaCeO_3$ but also in other perovskites, e.g., $BaPrO_3$ and $LaFeO_3$, that do not obey "the gradual tilting rule".

This work is supported by the Office of Naval Research Grants Nos. N00014-17-1-2818 and N00014-21-1-2086. H. X. is supported by the National Natural Science Foundation of China (Grants No. 11825403 and No. 11804138), and the Qing Nian Ba Jian Program.

---

* Corresponding author: laurent@uark.edu

[1] M. Trieloff, E. K. Jessberger, I. Herrwerth, J. Hopp, C. Fieni, M. Ghelis, M. Bourot-Denise, and P. Pellas, Nature **422**, 502 (2003).

[2] L. Bellaiche, A. García, and D. Vanderbilt, Phys. Rev. Lett. **84**, 5427 (2000).

[3] K. Ueda, H. Tabata, and T. Kawai, Science **280**, 1064 (1998).

[4] J. Wang, J. B. Neaton, H. Zheng, V. Nagarajan, S. B. Ogale, B. Liu, D. Viehland, V. Vaithyanathan, D. G. Schlom, U. V. Waghmare, N. A. Spaldin, K. M. Rabe, M. Wuttig, and R. Ramesh, Science **299**, 1719 (2003).

[5] R. J. Cava, B. Batlogg, R. B. van Dover, D. W. Murphy, S. Sunshine, T. Siegrist, J. P. Remeika, E. A. Rietman, S. Zahurak, and G. P. Espinosa, Phys. Rev. Lett. **58**, 1676 (1987).

[6] R. J. Cava, B. Batlogg, J. J. Krajewski, R. Farrow, L. W. Rupp Jr, A. E. White, K. Short, W. F. Peck, and T. Kometani, Nature **332**, 814 (1988).

[7] T. C. Jellicoe, J. M. Richter, H. F. Glass, M. Tabachnyk, R. Brady, S. E. Dutton, A. Rao, R. H. Friend, D. Credgington, N. C. Greenham, and M. L. Böhm, J. Am. Chem. Soc. **138**, 2941 (2016).

[8] M. W. Lufaso and P. M. Woodward, Acta Crystallogr., Sect. B **57**, 725 (2001).

[9] A. M. Glazer, Acta Crystallogr. Sect. B: Struct. Crystallogr. and Crystallogr. Chem. **28**, 3384 (1972).

[10] C. C. Stoumpos, C. D. Malliakas, J. A. Peters, Z. F. Liu, M. Sebastian, J. Im, T. C. Chasapis, A. C. Wibowo, D. Y. Chung, A. J. Freeman, B. W. Wessels, and M. G. Kanatzidis, Cryst. Growth Des. **13**, 2722 (2013).

[11] Y. He, C. C. Stoumpos, I. Hadar, Z. Luo, K. M. McCall, Z. Liu, D. Y. Chung, B. W. Wessels, and M. G. Kanatzidis, J. Am. Chem. Soc. **143**, 2068 (2021).

[12] K. S. Knight, G. D. Price, J. A. Stuart, and I. G. Wood, Phys. Chem. Miner. **42**, 45 (2014).

[13] S. Cuffini, J. A. Guevara, Y. P. Mascarenhas, P. de la Presa, A. Ayala, and A. L. Garcia, Cerâmica **43**, 91 (1997).

[14] C. J. Howard, K. S. Knight, B. J. Kennedy, and E. H. Kisi, J. Phys.: Condens. Matter **12**, L677 (2000).

[15] M. Yashima and R. Ali, Solid State Ionics **180**, 120 (2009).

[16] R. Ali and M. Yashima, J. Solid State Chem. **178**, 2867 (2005).

[17] B. J. Kennedy, C. J. Howard, and B. C. Chakoumakos, Phys. Rev. B **60**, 2972 (1999).

[18] B. J. Kennedy, A. K. Prodjosantoso, and C. J. Howard, J. Phys.: Condens. Matter **11**, 6319 (1999).

[19] L. Chen, B. Xu, Y. Yang, L. Bellaiche, Adv. Funct. Mat. **30**, 1909496, (2020).

[20] B. Xu, D. W. Wang, H. J. Zhao, J. Íñiguez, X. M. Chen, and L. Bellaiche, Adv. Funct. Mater. **25**, 3626 (2015).

[21] S. M. Selbach, J. R. Tolchard, A. Fossdal, and T. Grande, J. Solid State Chem. **196**, 249 (2012).

[22] P. J. Saines, B. J. Kennedy, and R. I. Smith, Mater. Res. Bull. **44**, 874 (2009).

[23] K. Knight, Solid State Ionics **74**, 109 (1994).

[24] K. Knight, Solid State Ionics **145**, 275 (2001).

[25] C. Zuo, S. Zha, M. Liu, M. Hatano, and M. Uchiyama, Adv. Mater. **18**, 3318 (2006).

[26] H. Iwahara, H. Uchida, K. Ogaki, and H. Nagato, J. Electrochem. Soc. **138**, 295 (1991).

[27] D. Medvedev, A. Murashkina, E. Pikalova, A. Demin, A. Podias, and P. Tsiakaras, Prog. Mater. Sci. **60**, 72 (2014).

[28] C. Ang, Z. Jing, and Z. Yu, J. Phys.: Condens. Matter **14**, 8901 (2002)

[29] L. P. Curecheriu, C. E. Ciomaga, V. Musteata, G. Canu, V. Buscaglia, and L. Mitoseriu, Ceram. Int. **42**, 11085 (2016).

[30] V. M. Goldschmidt, Naturwissenschaften **14**, 477 (1926).

[31] R. D. Shannon, Acta Cryst. A **32**, 751 (1976).

[32] W. Zhong, D. Vanderbilt, and K. M. Rabe, Phys. Rev. Lett. **73**, 1861 (1994); W. Zhong, D. Vanderbilt, and K. M. Rabe, Phys. Rev. B **52**, 6301 (1995).

[33] Y. Yang, B. Xu, C. Xu, W. Ren, and L. Bellaiche, Phys. Rev. B **97**, 174106 (2018).

[34] I. A. Kornev, L. Bellaiche, P. E. Janolin, B. Dkhil, and E. Suard, Phys. Rev. Lett. **97**, 157601 (2006).

[35] Z. Zhang, J. Koppensteiner, W. Schranz, J.B. Betts, A. Migliori and M.A. Carpenter, Phys. Rev. B **82**, 014113 (2010).

[36] S.-Y. Cheng, N.-J. Ho and H.-Y. Lu, J. Am. Ceram. Soc. **91**, 2298 (2008).

[37] S. Prosandeev, D. Wang, W. Ren, J. Íñiguez, and L. Bellaiche, Adv. Funct. Mater. **23**, 234 (2013).

[38] D. Albrecht, S. Lisenkov, W. Ren, D. Rahmedov, I. A. Kornev, and L. Bellaiche, Phys. Rev. B **81**, 140401(R) (2010).

[39] I. A. Kornev, S. Lisenkov, R. Haumont, B. Dkhil, and L. Bellaiche, Phys. Rev. Lett. **99**, 227602 (2007).

[40] S. Lisenkov, I. A. Kornev, and L. Bellaiche, Phys. Rev. B **79**, 012101 (2009).

[41] J. P. Perdew, A. Ruzsinszky, G. I. Csonka, O. A. Vydrov, G. E. Scuseria, L. A. Constantin, X.

Zhou, and K. Burke, Phys. Rev. Lett. **100**, 136406 (2008).

[42] G. Kresse and D. Joubert, Phys. Rev. B **59**, 1758 (1999).

[43] P. E. Blochl, Phys. Rev. B **50**, 17953 (1994).

[44] J. F. Nye, Physical Properties of Crystals, Their Representation by Tensors and Matrices, Clarendon Press, Oxford 1957.

[45] A. M. George, J. Íñiguez and L. Bellaiche, Phys. Rev. B **65**, 180301(R) (2002).

[46] L. Bellaiche, and J. Íñiguez, Phys. Rev. B **88**, 014104 (2013).

[47] E. Bousquet, M. Dawber, N. Stucki, C. Lichtensteiger, P. Hermet, S. Gariglio, J. M. Triscone, and P. Ghosez, Nature **452**, 732 (2008).

[48] J. M. Rondinelli and C. J. Fennie, Adv. Mater. **24**, 1961 (2012).

[49] N. A. Benedek and C. J. Fennie, Phys. Rev. Lett. **106**, 107204 (2011).

[50] A. V. Kuzmin, V. P. Gorelov, B. T. Melekh, M. Glerup, and F. W. Poulsen, Solid State Ionics **162**, 13 (2003).

[51] T. Ohzeki, S. Hasegawa, M. Shimizu, and T. Hashimoto, Solid State Ionics **180**, 1034 (2009).

[52] F. Bertolotti, L. Protesescu, M. V. Kovalenko, S. Yakunin, A. Cervellino, S. J. L. Billinge, M. W. Terban, J. S. Pedersen, N. Masciocchi, and A. Guagliardi, ACS Nano **11**, 3819 (2017).

[53] J. Klarbring, Phys. Rev. B **99**, 104105 (2019).

[54] S.-Y. Cheng, N.-J. Ho, and H.-Y. Lu, J. Am. Ceram. Soc. **89**, 3498 (2006).

[55] T. Scherban, R. Villeneuve, L. Abello, and G. Lucazeau, J. Raman Spectrosc. **24**, 805 (1993).

[56] S. Loridant, L. Abello, E. Siebert, and G. Lucazeau, Solid State Ionics **78**, 249 (1995).

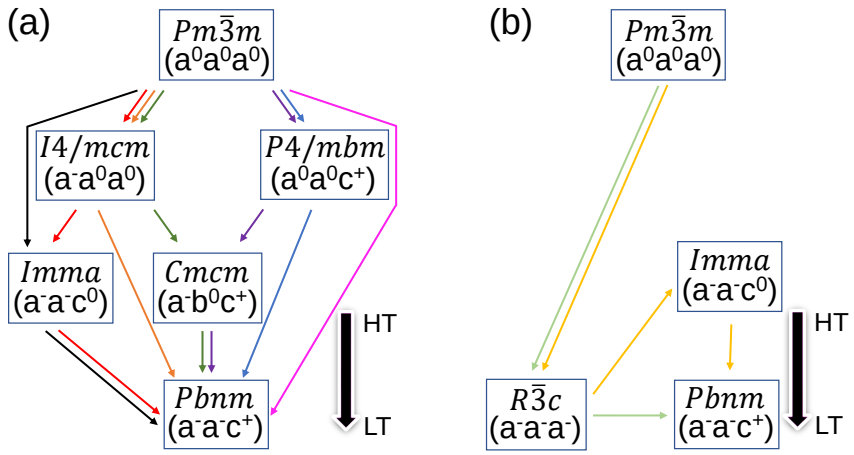

FIG. 1: Different known possibilities to go from the $Pm\bar{3}m$ state ($a^0a^0a^0$ in Glazer notations) at high temperature (HT) to the $Pbnm$ state ($a^-a^-c^+$ in Glazer notations) at low temperature (LT). Panel (a) depicts the possibilities that are consistent with "the gradual tilting rule", while Panel (b) shows solutions that violate this rule.

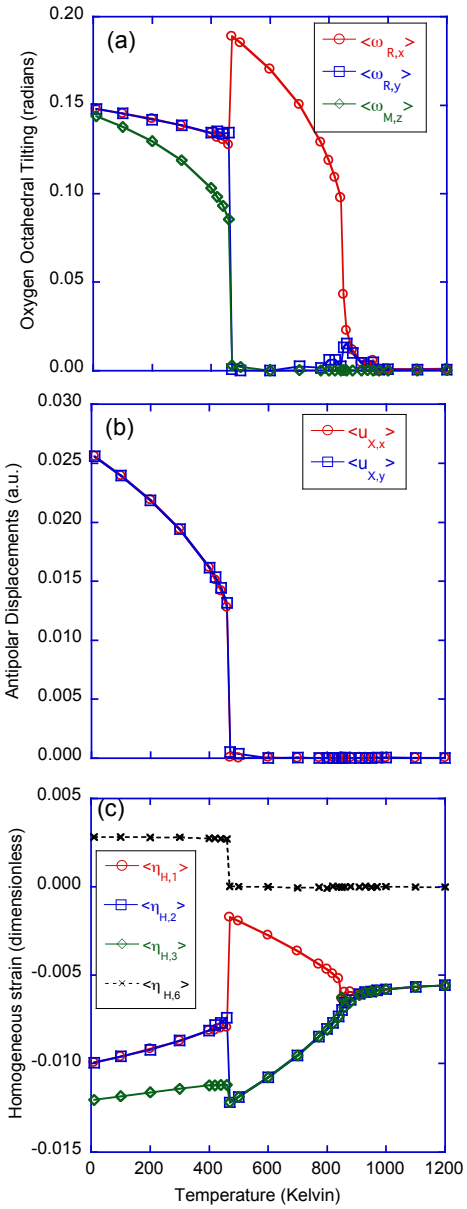

FIG. 2: Temperature dependency of some physical properties of $BaCeO_3$ bulk and monodomain, as predicted by the presently developed effective Hamiltonian with its *ab-initio* parameters: (a) the x- and y-components of the antiphase-tilting-related $< \omega_{\mathbf{R}} >$ and the z-component of the in-phase-tilting-related $< \omega_{\mathbf{M}} >$; (b) the x- and y-components of the antipolar-related $< \mathbf{u_X} >$; and (c) $\eta_{H,1}$, $\eta_{H,2}$, $\eta_{H,3}$ and $\eta_{H,6}$ homogeneous strain components. The components of $< \omega_{\mathbf{R}} >$, $< \omega_{\mathbf{M}} >$, $< \mathbf{u_X} >$ and $\{\eta_H\}$ that are not shown here are null for any temperature.

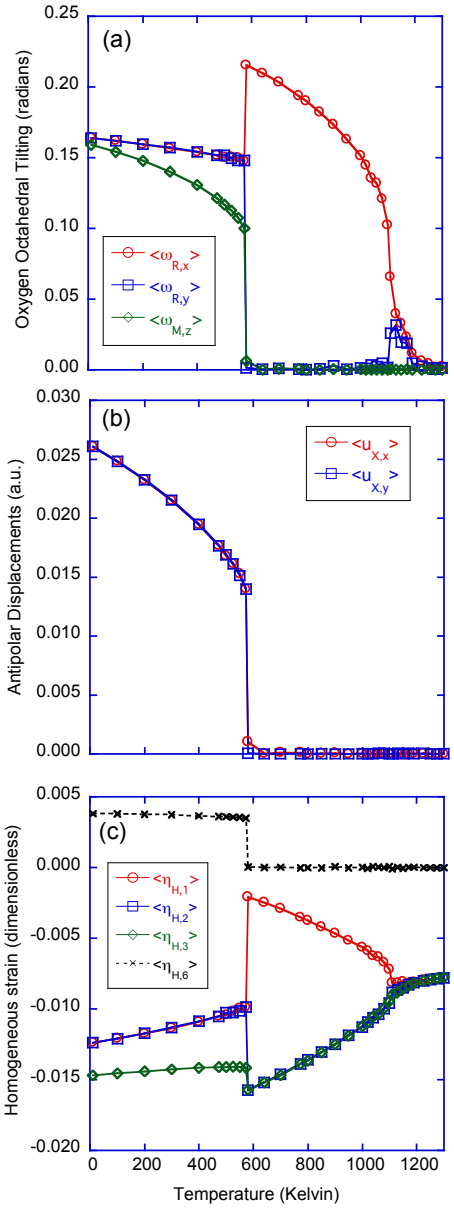

FIG. 3: Same as Figure 2, but with the κ_A parameter being varied from its *ab-initio* value of -0.138305 to -0.208305.

TABLE 1: Expansion parameters of the effective Hamiltonian for $BaCeO_3$ from first principles. Atomic units are used here. The reference cubic lattice parameter is 8.353 Bohr.

Dipole	Z^*	+4.0704	ϵ_∞	+5.378	
u on-site	κ_2	+0.007524	α	+0.00604	γ +0.00305
u short range	j_1	-0.0016861	j_2	+0.00290598	
	j_3	+0. 00023602	j_4	-0.00031182	j_5 -0.00059289
	j_6	+0.000120581	j_7	+0.00006029	
Elastic	B_{11}	+2.9506	B_{12}	+0.9785	B_{44} +0.6213
u-strain coup.	B_{1xx}	-0.14126	B_{1yy}	+0.00406	B_{4yz} -0.02683
ω on-site	κ_A	-0.138305	α_A	+2.7315847	γ_A -0.3338634
ω short-range	k_1	+0.03457625	k_2	+0.008665	K' +0.02867875
ω-strain coup.	C_{1xx}	+0.38	C_{1yy}	+1.0695	C_{4yz} +0.27196
ωu coup. (trilinear)	$D_{ii,xy}$	-0.0437584			
ωu coup. (bi-quadratic)	E_{xxxx}	+0.384118	E_{xxyy}	+0.226458	E_{xyxy} -0.319028